Beam Flux Measurement Using Photon Activation Analysis Method at SLEGS*

Yu-Xuan Yang,[1,2] Yue Zhang,[3] Zhi-Cai Li,[4,3] Zi-Rui Hao,[3] Sheng Jin,[2,5] Kai-Jie Chen,[2,6] Zhen-Wei Wang,[2,5] Qian-Kun Sun,[2,5] Gong-Tao Fan,[3,2,5] Hang-Hua Xu,[3] Long-Xiang Liu,[3] Wei-Juan Zhao,[1,†] and Hong-Wei Wang[3,2,5,‡]

[1]*School of Physics and Microelectronics, Zhengzhou university, Zhengzhou 450001 China*
[2]*Shanghai Institute of Applied Physics, Chinese Academy of Sciences, Shanghai 201800, China*
[3]*Shanghai Advanced Research Institute, Chinese Academy of Sciences, Shanghai 201210, China*
[4]*School of Nuclear Science and Technology, University of South China, Hengyang 421001, China*
[5]*University of Chinese Academy of Sciences, Beijing 100049, China*
[6]*School of Physical Science and Technology, ShanghaiTech University Shanghai 201210, China*

The Shanghai Laser Electron Gamma Source(SLEGS) has delivered a quasi-monochromatic, continuously energy-tunable γ-ray beam. Based on the photon activation analysis(PAA) method, SLEGS has built and developed a photon activation analysis platform, including online activation and offline low-background HPGe detector measurement systems, as an alternative to direct measurement methods and a cross-tests at low throughput. Due to the short half-lives spanning from minutes to days and characteristics such as ease of fabrication, cost-effectiveness, and stability, gold (^{197}Au) and zinc (^{64}Zn) emerge as favorable activation targets in the γ-ray beam flux monitor. Notably, their utility shows a multitude of advantages in monitoring the γ-ray beam flux typically 10^5 photons/s with the energy of 13.16 to 19.08 MeV u nder the condition of the 3 mm coarse collimator. Especially in high-flux γ-ray beam experiments can be well applied.

Keywords: SLEGS, Laser Compton Scattering, Beam Flux, Photon Activation Analysis

I. INTRODUCTION

The Shanghai Laser Electron Gamma Source (SLEGS) is one of the beamline stations constructed in the Shanghai Synchrotron Radiation Facility (SSRF) Project II. SLEGS as the first pioneering Laser Compton Slanting Scattering (LCSS) Gamma Source is characterized by its innovative approach of employing a continuously changing collision angle from 20 to 160 degrees, which can produce adjustable γ-ray energy within the range of 660 keV to 21.7 MeV [1, 2]. SLEGS is an important platform for basic and applied science research in photonuclear physics.

The γ-ray beam flux stands out as a crucial parameter for SLEGS, and its measurement can be accomplished through direct or indirect methods. Large-volume scintillator detectors, such as $LaBr_3(Ce)$, BGO, and NaI, offer direct measurement of γ-ray energy. However, limitations arise in high count rates (less than 10^6 cps) due to the long decay time of scintillators and the limited readout rate of PMTs. Plastic scintillator paddle detectors, employed at HIγS, allow beam flux measurement up to 3×10^7 photons/s with an accuracy of at least 2% [3].

At SLEGS, direct measurements are facilitated by a large-sized NaI detector with a diameter of $\Phi 203.2\,\mathrm{mm} \times 304.8\,\mathrm{mm}$, directly readout by four PMTs. Additionally, a large volume $\Phi 76.2\,\mathrm{mm} \times 101.6\,\mathrm{mm}$ $LaBr_3(Ce)$ detector [4] and a $\Phi 76.2\,\mathrm{mm} \times 200\,\mathrm{mm}$ BGO detector are employed for direct monitoring of the attenuated beam. Indirect methods rely on nuclear reactions induced by γ-rays, such as $d(\gamma, n)p$ in D_2O and Deuterated Benzene Cell (C_6D_6) targets, used to monitor the beam flux by counting neutrons at HIγS. The γ-ray flux calculated at 3 MeV is 1.2×10^7 photons/s with the simulation detector efficiency, and the overall systematic uncertainty can be limited to below 5% [5, 6]. Another indirect method involves Compton scattering by a copper target, to be employed at ELI-NP for measuring relative beam flux [7]. Additionally, the photon activation method, which involves photonnuclear reactions such as $^{197}\mathrm{Au}(\gamma, \mathrm{n})^{196}\mathrm{Au}$, $^{27}\mathrm{Al}(\gamma, \mathrm{x})^{24}\mathrm{Na}$, $^{93}\mathrm{Nb}(\gamma, \mathrm{n})^{92\mathrm{m,g}}\mathrm{Nb}$, and others, serves as a third approach for determining the beam flux. Specifically, for LLCS γ-ray beams at SLEGS, $^{197}\mathrm{Au}(\gamma, \mathrm{n})^{196}\mathrm{Au}$ and $^{64}\mathrm{Zn}(\gamma, \mathrm{n})^{63}\mathrm{Zn}$ have been selected to measure the γ-ray beam flux.

This article is organized as follows, section 2 gives the basic principles and methods introduction of Photon Activation Analysis(PAA) [8, 9], including the γ-ray beam source and the detection system. Section 3 reviews the data analysis procedures. Section 4 discusses the future prospects of PAA, such as the improvement of nuclear reaction data, the development of new γ-ray sources and the integration of PAA with other techniques.

II. SLEGS BEAMLINE AND PAA SETUP

A. γ-ray beam characterization

A Laser Compton scatter γ-ray beam was generated at the interaction chamber by employing a 10.64 μm wavelength

* This work was supported by the National key RD program(No.2022YFA1602404),the National Natural Science Foundation of China (No. 12275338, No. 12005280, No. 11975210), the Key Laboratory of Nuclear Data foundation (JCKY2022201C152) and the Chinese Academy of Sciences President's International Fellowship Initiative(No. 2021VMA0025)

† Corresponding author, Wei-Juan Zhao, E-mail: zwj@zzu.edu.cn
‡ Corresponding author, Hong-Wei Wang, E-mail: wanghw@sari.ac.cn

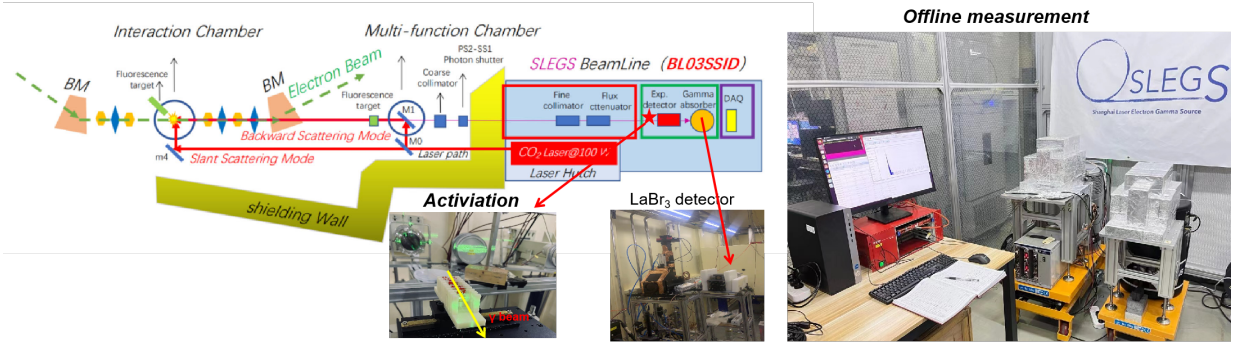

Fig. 1. Schematic layout of the SLEGS beamline, online activation, and offline low background HPGe setup.

CO_2 laser operating at 1 kHz low frequency and 50 μs pulse width (equivalent to 5 W laser power). This laser beam collided with a 3.5 GeV electron in the SSRF storage ring, resulting in the production of quasi-monochromatic γ-rays with energy varying from 0.25 to 21.7 MeV. The γ-ray beam flux ranged between 4.8×10^5 and 1.5×10^7 ph/s. The LCSS γ-ray beam was then directed through a vacuum pipeline, traversing a coarse collimator, fine collimator, and attenuator [10–12], before ultimately reaching the experimental hutch. This well-controlled transport setup ensures the precise delivery of the γ-ray beam to the experimental room.

A diagram illustrating the online activation and offline measurements is presented in Fig. 1. The activation platform, featuring a multi-slot target holder, is strategically positioned behind the beam pipe exit. To facilitate beam spot imaging and reaction target localization, a silicon pixel imaging detector (MiniPIX) is employed. Additionally, a $\Phi76.2\,\mathrm{mm}\times101.6\,\mathrm{mm}$ $LaBr_3(Ce)$ detector is placed at the termination point of the LCS γ-ray beamline to measure both the γ-ray beam flux and energy. Fig. 2 shows the detector response to γ-ray beam at different collision angles of 124° and 132° using 3 mm coarse collimator under 200 mm copper attenuation. The profile of quasi-monoenergetic γ-ray overlay on continuous bremsstrahlung background is clearly visible. Utilizing the unfolding method, the corresponding gamma energy spectrum without the detector response was successfully solved as shown in Fig. 2(pink line and blue line). A paper detailing the unfolding of γ-ray beam is currently in preparation [13].

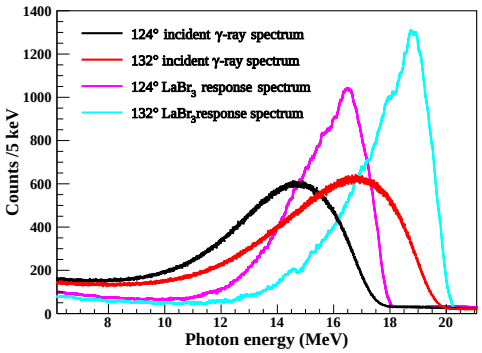

Fig. 2. The γ-ray energy spectrum measured with a $\Phi76.2\,\mathrm{mm}\times101.6\,\mathrm{mm}$ $LaBr_3(Ce)$ detector and the spectrum were solved by unfolding method. γ-ray energy spectrum of several laser-electron collision angles measured by $LaBr_3(Ce)$ detector for 124°(black) and 132°(red). Unfolding γ-ray energy spectrum at the same angles.

B. The low background HPGe detector system

The measurement of characteristic γ-rays emitted from the sample of the nuclide under study is conducted using an HPGe detector (ORTEC GEM70200-p). This detector boasts a relative efficiency of 55.2% at 1333 keV and an impressive energy resolution of 5.99 keV at 1333 keV (0.45%). To minimize background interference, 10 cm thick lead shields are employed, ensuring low background counts of less than 5 cps within the 60 keV to 3000 keV region.

Calibration of the HPGe detector efficiency is meticulously carried out using standard gamma sources, including ^{152}Eu (24.5 kBq), ^{137}Cs (8.177 kBq), ^{57}Co (80.73 kBq), and ^{241}Am (6.516 kBq). The absolute efficiency (η) for the gamma source, positioned at the same distance from the HPGe detector, is determined by the expression given in Eq. (1). This rigorous calibration ensures accurate and reliable measurements of the irradiated target's activity.

$$\eta = \frac{NF_{tsc}}{A_0 e^{-\lambda T} I_\gamma T_c} \tag{1}$$

In the expression, N represents the photon peak counts obtained for the characteristic γ-rays of ^{152}Eu, ^{57}Co, ^{137}Cs, and ^{60}Co. A_0 stands for the source activity at the factory, T is the time elapsed from the factory to the present, I_γ denotes the characteristic γ-ray transition relative intensity, and T_c is the counting time. The correction factor for the coincidence summing effect is denoted as F_{tsc}. To estimate the efficiencies corresponding to the γ-rays emitted from the decay of ^{152}Eu, ^{57}Co, ^{137}Cs, and ^{60}Co, a linear parametric model represented by Eq. (2) is employed.

The fitted curve of the interpolated detector efficiency and the measured detector efficiency are visualized in Fig 3. Furthermore, the correction for summing coincidence effects is

accomplished through Geant4 simulation [14], ensuring accurate corrections and enhancing the reliability of the calibration process.

$$\epsilon = e^{a+blnE+clnE^2+dlnE^3+elnE^4+flnE^5}, \quad (2)$$

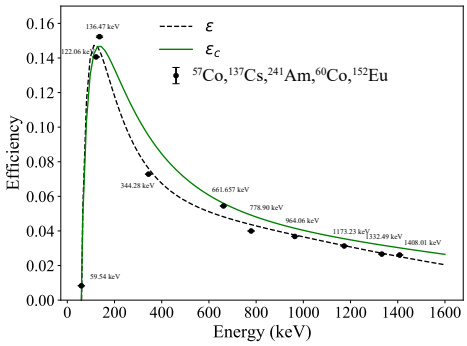

Fig. 3. Measured detector efficiency along with interpolated detector efficiency fitting curve.

III. ACTIVATION DATA ANALYSIS

Gold, being a commonly utilized activated material, was chosen for comparison with zinc, a short-lived activated material. In the present work, the γ-ray beam flux extracted from the $^{197}\mathrm{Au}(\gamma,\mathrm{n})^{196}\mathrm{Au}$ and $^{64}\mathrm{Zn}(\gamma,\mathrm{n})^{63}\mathrm{Zn}$ reactions was meticulously measured at SLEGS. The measurements spanned from 102° (13.16 MeV) to 139° (19.08 MeV), providing valuable insights into the characteristics of the beam flux.

A. Calculation of the γ-ray beam flux

The γ-ray beam flux $\phi(E_\gamma)$ (1/s) was determined by the activation Eq. (3)

$$\phi_{E_\gamma} = \frac{N_\gamma}{\sigma(E_\gamma)N_A A_b I_\gamma \eta f_t f_s} \quad (3)$$

Here, N_γ is effective counts measured by the HPGe detector, A_b is the natural isotope abundance of the target. The time correction factor f_t is shown below

$$f_t = \frac{(1-e^{-\lambda T_i})e^{-\lambda T_w}(1-e^{-\lambda T_c})}{\lambda} \quad (4)$$

Where λ(1/s) is the decay constant. $\mathrm{T_i}$ is the irradiation time, and T_w,called as cooling time, is the elapsed waiting time between the end of irradiation and the start of the offline HPGe measurement count.

The self-attenuation coefficients f_s due to the interactions of γ-rays within the sample thickness is given by Eq. 5

$$f_s = \frac{\mu t}{1-e^{-\mu t}} \quad (5)$$

B. Target material for activation

The $^{197}\mathrm{Au}(\gamma,\mathrm{n})^{196}\mathrm{Au}$ and $^{64}\mathrm{Zn}(\gamma,\mathrm{n})^{63}\mathrm{Zu}$ reactions have been specifically chosen to serve as monitors for the γ-ray beam flux in SLEGS. The single-neutron outgoing thresholds for $^{197}\mathrm{Au}$ and $^{64}\mathrm{Zn}$ are 8.073 MeV and 11.86 MeV, respectively. Consequently, the γ-ray beam flux can be effectively monitored within the energy ranges of 8.07-21.00 MeV and 11.96-25.00 MeV for these reactions, ensuring comprehensive coverage across the desired γ-ray beam energies. They exhibit a broader monitoring energy range.The giant resonance excitation functions for these reactions are depicted in Fig. 4(a) and (b), respectively. This presentation encompasses both previously reported experimental data from the EXFOR database and evaluated cross-section data from the ENDF/B VIII and IAEA-2019 libraries. With their substantial cross-sections, these reactions facilitate short activation times, making them versatile for a variety of experiments. The half-lives of $^{196\mathrm{g}}\mathrm{Au}$ and $^{63}\mathrm{Zn}$ are 6.1669 days and 38.47 minutes, respectively.

Fig. 5 illustrates the level scheme of $^{196\mathrm{g}}\mathrm{Au}$ decay and $^{63}\mathrm{Zn}$ decay, along with the characteristic γ-ray energies and intensities associated with each. Relative nuclear spectroscopic data were sourced from the NuDat 3.0 database [15]. Both reactions are well-suited for offline measurements, adding to their utility in experimental settings.

The beam flux activation monitor utilized a natural gold target (^{197}Au 100%) with a purity of 99.99% and a thickness of 0.5 mm. Additionally, a natural zinc target (^{64}Zn 49.2%, ^{66}Zn 27.7%, ^{67}Zn 4.0%, ^{68}Zn 18.5%, ^{70}Zn 0.6%) with 99.99% purity and 2 mm thickness was employed. The target had a diameter of 10 mm, exceeding the diameter of the γ-ray beam restricted by a 3 mm coarse collimator. Strategically situated on a multi-slot target holder along the beam axis, precisely positioned in front of the experimental hutch, the target underwent meticulous irradiation by a focused γ-ray beam. This deliberate irradiation served for the well-controlled $^{197}\mathrm{Au}(\gamma,\mathrm{n})^{196}\mathrm{Au}$ and $^{64}\mathrm{Zn}(\gamma,\mathrm{n})^{63}\mathrm{Zn}$ reaction, playing a crucial role in the experimental procedure.

$^{197}\mathrm{Au}(\gamma,\mathrm{n})^{196}\mathrm{Au}$ reaction resulted in the production of the unstable nuclei $^{196\mathrm{m}}\mathrm{Au}$ and $^{196\mathrm{g}}\mathrm{Au}$. Subsequently, $^{196\mathrm{m}}\mathrm{Au}$ underwent de-excitation by emitting γ-rays, leading to the formation of $^{196\mathrm{g}}\mathrm{Au}$. The decay of $^{196\mathrm{g}}\mathrm{Au}$ proceeded through either electron capture (93%), yielding ^{196}Pt, or β^- decay (7%), resulting in ^{196}Hg. The decay profile is visualized in Fig 5(a). while additional reaction details are summarized in Table1.

Table 1. Isotope and Decay data.

product nuclide	Reaction	S_n (MeV)	$T_{1/2}$	E_γ(keV)	I_γ
^{196g}Au	^{197}Au$(\gamma,n)^{196}$Au	8.073	6.1669 day	355.73	0.87
^{63}Zn	^{64}Zn$(\gamma,n)^{63}$Zn	11.86	38.47 min	511.00	1.855

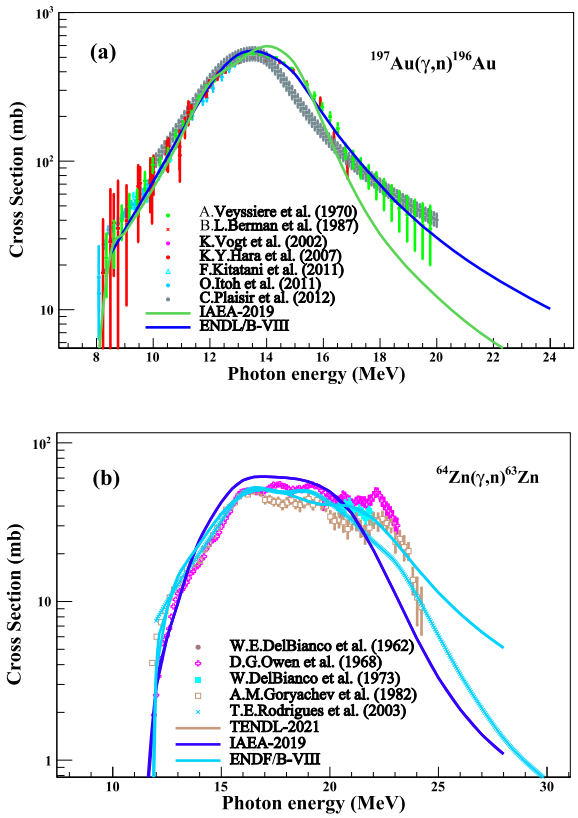

Fig. 4. (a) ^{197}Au$(\gamma,n)^{196}$Au cross section as function of γ-ray energy from the literature [16–24] as well as evaluated data ENDF/B-VIII and IAEA-PD-2019. (b) ^{64}Zn$(\gamma,n)^{63}$Zn cross section as function of γ-ray energy from the literature [25–31] as well as evaluated ENDF/B-VIII and IAEA-PD-2019 [32].

C. Characteristic γ-ray de-excitation spectrum

The γ-ray beam flux was quantified through the identification of characteristic transition peaks associated with the ground state of ^{196g}Au, following the photon-neutron reaction with ^{197}Au. This ground state of ^{196g}Au possesses a half-life of 6.1669 days, making it a reliable marker for assessing the strength of the γ-ray beam. The irradiation, cooling, and counting times were carefully chosen: $t_i = 0.5637$ days for irradiation, $T_w = 2.24$ days for cooling, and $T_c = 224,309$ seconds for counting. Notably, the cooling time exceeds two days, ensuring a 99% decay of the excited state of ^{196m}Au (E_{level}=0.5957 MeV, $T_{1/2}$=9.6 hours) to reach the ground state. This meticulous time allocation enhances the reliability and precision of the experimental measurements.The distinct characteristic γ-ray transitions resulting from the irradiation of the ^{197}Au target with a 19.08 MeV γ-ray beam are clearly evident in Fig 5(a). Notably, the characteristic γ-rays of ^{196g}Au include peaks at 355.73 keV and 333.03 keV, originating from the $\beta-$ decay of ^{196g}Au, along with a peak at 426.10 keV corresponding to the transition (IT) decay of ^{196g}Au. These features contribute to a comprehensive understanding of the experimental spectrum.

For ^{63}Zn, it undergoes β^+ decay, resulting in the emission of a characteristic peak at 511 keV due to the annihilation of positrons with electrons. The gamma-ray spectrum recorded for Zinc samples irradiated with 19.08 MeV photons is illustrated in Fig. 5(b). The experimental conditions included an irradiation time of $t_i = 2$ hours, a cooling period of $T_w = 3.1$ minutes, and a counting time of $T_c = 2$ hours. Notably, the statistical errors associated with these measurements are all below 1%, highlighting the precision of the experimental data.

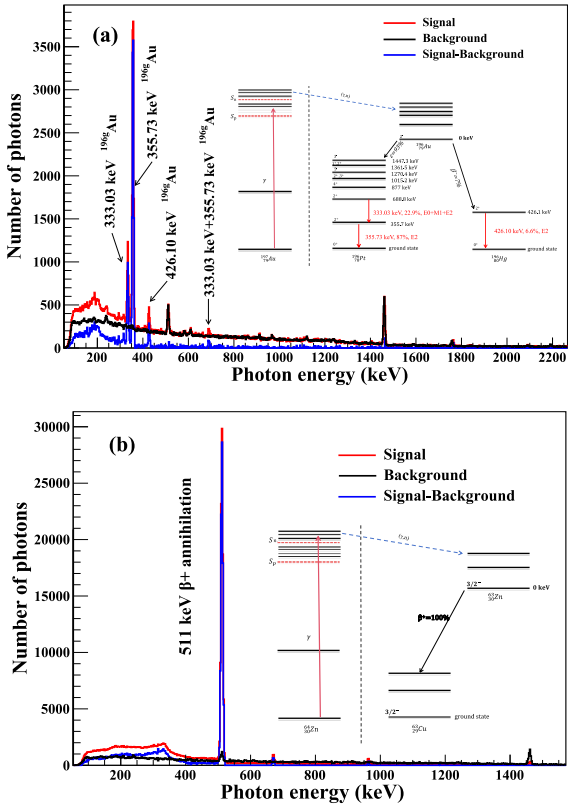

Fig. 5. The typically recorded spectra for the Au and Zn sample irradiated by 19.08 MeV.

IV. RESULTS AND DISCUSSION

The γ-ray beam flux was determined through the activation reactions $^{197}\mathrm{Au}(\gamma,\mathrm{n})^{196\mathrm{g+m}}\mathrm{Au}$ and $^{64}\mathrm{Zn}(\gamma,\mathrm{n})^{63}\mathrm{Zu}$, as well as direct measurements using a $\mathrm{LaBr_3(Ce)}$ detector. The results, presented in Fig 6, obtained from the activation reactions, exhibited excellent agreement with the $\mathrm{LaBr_3(Ce)}$ detector results and Geant4 simulation outcomes.

Under the conditions of a 3 mm coarse collimator aperture, the γ-ray beam flux ranged from 1.8×10^5 photons/s to 7×10^5 photons/s, varying with the collision angle between the laser and electron beam (ranging from 102° to 139°, corresponding to γ-ray beam energies of 13.16-19.08 MeV). This substantiates the reliability and convenience of the photon activation analysis method, proving it to be as effective as classical beam monitoring methods. When utilizing suitable short-lived target materials, this approach allows for sensitive and rapid online monitoring across different energy regions.

At higher γ-ray beam flux levels, direct monitoring becomes challenging. In such cases, photon activation monitoring serves as an excellent means of flux indexing. Our group has also developed a rapid monitoring method for short-lived target materials, as detailed in subsequent references. The total uncertainties in the measured γ-ray beam flux for the $^{197}\mathrm{Au}(\gamma,\mathrm{n})^{196\mathrm{g+m}}\mathrm{Au}$, $^{64}\mathrm{Zn}(\gamma,\mathrm{n})^{63}\mathrm{Zu}$ reactions, and $\mathrm{LaBr_3(Ce)}$ detector are listed in Table 2.

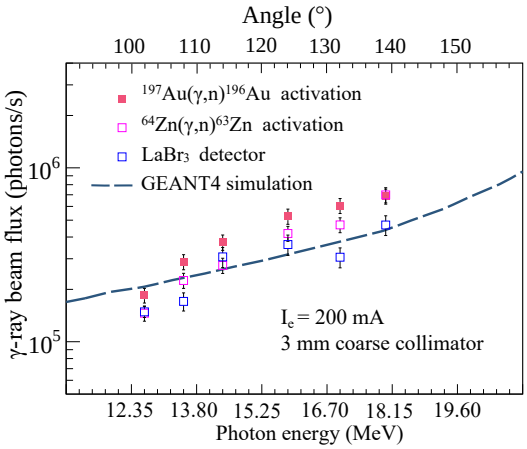

Fig. 6. γ-ray beam flux results from $^{197}\mathrm{Au}(\gamma,\mathrm{n})^{196\mathrm{g+m}}\mathrm{Au}$ and $^{64}\mathrm{Zn}(\gamma,\mathrm{n})^{63}\mathrm{Zu}$ reaction, also compared with $\mathrm{LaBr_3(Ce)}$ detector direct measurement and Geant4 simulation

The error analysis for the γ-ray beam flux measurement encompasses several factors. These include the statistical error of the characteristic γ-ray counts (ϵ_{N_γ}), the relative errors of decay constants (ϵ_λ) taken from literature (0.01%) [33], and the uncertainty in the $^{197}\mathrm{Au}(\gamma,\mathrm{n})^{196\mathrm{g+m}}\mathrm{Au}$ and $^{64}\mathrm{Zn}(\gamma,\mathrm{n})^{63}\mathrm{Zu}$ cross-sections, which is negligible as indicated in Fig. 4. However, there is a significant error in the experimentally measured cross-sections for the two reaction channels, some exceeding 10%. To mitigate this, we adopt the IAEA data from the evaluation database as the standard cross-sectional value in data analysis.

The efficiency calibration relative errors of the HPGe detector are denoted as ϵ_η, and the relative errors of the number of targets per unit area (ϵ_{N_A}) are associated with the thickness of targets. Given that the experiment's timing has confidence in the picosecond range, as compared to irradiation time intervals of at least hours, ϵ_T is considered negligible. The corresponding results are presented in Table 2.

Table 2. the statistical error in PAA method be used.

Reaction	ϵ_{N_γ} [%]	ϵ_λ [%]	ϵ_{N_A} [%]	ϵ_{I_γ} [%]	ϵ_η [%]
$^{197}\mathrm{Au}(\gamma,\mathrm{n})^{196\mathrm{g+m}}\mathrm{Au}$	0.69	0.01	0.71	0.028	3.71
$^{64}\mathrm{Zn}(\gamma,\mathrm{n})^{63}\mathrm{Zn}$	0.72	0.13	0.05	0.09	3.71

V. CONCLUSION

A flux monitoring system utilizing the photon activation analysis (PAA) method has been developed at for SLEGS. This system serves as a supplementary and cross-checking tool for direct measurements. The monitoring system comprises both online activation and offline low-background HPGe detector components. In this setup, natural materials such as Gold (Au) and Zinc (Zn) have been selected as preferred target materials. This choice is based on the relatively short half-lives of $^{196\mathrm{g}}\mathrm{Au}$ and $^{63}\mathrm{Zn}$, which renders them stable for use at γ-ray flux levels exceeding 10^5 photons/s. The chosen materials are effective within the energy range of 13.16-19.08 MeV. This system proves particularly beneficial for high-flux γ-ray beam experiments.

The SLEGS activity platform, through this newly established flux monitoring system, enhances experimental capabilities. This enhancement makes it well-suited for conducting photoneutron cross-section measurements using quasi-monochromatic energy γ-ray beams.

Author Contributions: All authors contributed to the study's conception and design. Material preparation, data collection, and analysis were performed by Y-X Yang. The first draft of the manuscript was written by Y-X Yang and H-W Wang, and all authors commented on previous versions of the manuscript. All authors read and approved the final manuscript.

ACKNOWLEDGMENTS

The authors would thank the SSRF colleagues of the accelerator department and the beamline engineering department for their technical support and assistance.

[1] H. W. Wang, G. T. Fan, L. X. Liu, H. H. Xu, W. Q. Shen, Y. G. Ma, H. Utsunomiya, L. L. Song, X. G. Cao, Z. R. Hao, K. J. Chen, S. Jin, Y. X. Yang, X. R. Hu, X. X. Li, P. Kuang, Commissioning of laser electron gamma beamline slegs at ssrf, Nuclear Science and Techniques 33 (7) (2022) 87. doi:10.1007/s41365-022-01076-0.

[2] K. J. Chen, L. X. Liu, Z. R. Hao, Y. G. Ma, H. W. Wang, G. T. Fan, X. G. Cao, H. H. Xu, Y. F. Niu, X. X. Li, X. R. Hu, Y. X. Yang, S. Jin, P. Kuang, Simulation and test of the SLEGS TOF spectrometer at SSRF, Nuclear Science and Techniques 34 (3) (2023) 47. doi:10.1007/s41365-023-01194-3.

[3] R. Pywell, O. Mavrichi, W. Wurtz, R. Wilson, Photon flux monitor for a mono-energetic gamma ray source, Nuclear Instruments and Methods in Physics Research Section A: Accelerators, Spectrometers, Detectors and Associated Equipment 606 (3) (2009,7) 517–522. doi:10.1016/j.nima.2009.04.014.

[4] Saint-gobain, https://www.crystals.saint-gobain.com.

[5] C. Matei, J. Mueller, M. Sikora, G. Suliman, C. Ur, H. Weller, Investigation of the d(γ,n)p reaction for gamma beam monitoring at eli-np, Journal of Instrumentation 11 (05) (2016) P05025–P05025. doi:10.1088/1748-0221/11/05/P05025.

[6] A. Banu, E. G. Meekins, J. A. Silano, H. J. Karwowski, S. Goriely, Photoneutron reaction cross section measurements on mo 94 and zr 90 relevant to the p -process nucleosynthesis, Physical Review C 99 (2) (2019) 025802. doi:10.1103/PhysRevC.99.025802.

[7] G. Turturica, C. Matei, A. Pappalardo, D. Balabanski, S. Chesnevskaya, V. Iancu, C. Ur, H. Karwowski, K. Chipps, M. Febbraro, S. Pain, D. Walter, C. Diget, J. Frost-Schenk, M. Munch, G. Guardo, M. La Cognata, R. Pizzone, G. Rapisarda, K. Chae, M. Kim, M. Kwag, Investigation of compton scattering for gamma beam intensity measurements and perspectives at eli-np, Nuclear Instruments and Methods in Physics Research Section A: Accelerators, Spectrometers, Detectors and Associated Equipment 921 (2019) 27–32. doi:Photoactivationexperimentof.

[8] C. Segebade, A. Berger, Photon Activation Analysis, Encyclopedia of Analytical Chemistrydoi:10.1002/9780470027318.a6211.pub2.

[9] C. Segebade, V. N. Starovoitova, T. Borgwardt, D. Wells, Principles, methodologies, and applications of photon activation analysis: a review, Journal of Radioanalytical and Nuclear Chemistry 312 (3) (2017) 443–459. doi:10.1007/s10967-017-5238-6.

[10] Z. R. Hao, G. T. Fan, H. W. Wang, L. X. Liu, H. H. Xu, H. Utsunomiya, X. G. Cao, B. J. Xu, L. L. Song, X. R. Hu, X. X. Li, Y. X. Yang, P. Kuang, Collimator system of slegs beamline at shanghai light source, Nuclear Instruments and Methods in Physics Research Section A: Accelerators, Spectrometers, Detectors and Associated Equipment 1013 (2021) 165638. doi:10.1016/j.nima.2021.165638.

[11] Z. R. Hao, G. T. Fan, H. W. Wang, H. H. Xu, L. X. Liu, L. L. Song, X. R. Hu, X. X. Li, P. Kuang, S. Jin, A new annular collimator system of slegs beamline at shanghai light source, Nuclear Instruments and Methods in Physics Research Section B: Beam Interactions with Materials and Atoms 519 (2022) 9–14. doi:10.1016/j.nimb.2022.02.010.

[12] H. H. Xu, G. T. Fan, H. W. Wang, H. Utsunomiya, L. X. Liu, Z. R. Hao, H. L. Wu, L. L. Song, Q. L. Zhang, B. C. Jiang, X. R. Hu, X. X. Li, P. Kuang, Y. X. Yang, S. Jin, Interaction chamber for laser compton slant-scattering in slegs beamline at shanghai light source, Nuclear Instruments and Methods in Physics Research Section A: Accelerators, Spectrometers, Detectors and Associated Equipment 1033 (2022) 166742. doi:PhotonuclearreactionsâĂŤFrombasic.

[13] L. Liu, H. Utsunomiya, G. Fan, H. Xu, H. Wang, Z.R.Hao, Y. Zhang, C. He, P. Jiao, S. Ye, S. Jin, K. Chen, Y. Yang, Q. Sun, Z. Wang, Z. Li, M. Zhou, X. Lu, C. Yang, F. Lu, X. Cao, Direct unfolding of total-energy responses of a 76 mm*200 mm bgo detector into gamma-ray energy distributions (Apr. 2023).

[14] L. C. He, L. J. Diao, B. H. Sun, L. H. Zhu, J. W. Zhao, M. Wang, K. Wang, Summing coincidence correction for γ -ray measurements using the hpge detector with a low background shielding system, Nuclear Instruments and Methods in Physics Research Section A: Accelerators, Spectrometers, Detectors and Associated Equipment 880 (2018) 22–27. doi:10.1016/j.nima.2017.09.043.

[15] National nuclear data center nudat 3.0, https://www.nndc.bnl.gov/nudat3/.

[16] C. Plaisir, F. Hannachi, F. Gobet, M. Tarisien, M. M. Aléonard, V. Méot, G. Gosselin, P. Morel, B. Morillon, Measurement of the 85rb(γ, n)84mrb cross-section in the energy range 10-19 mev with bremsstrahlung photons, The European Physical Journal A 48 (5) (2012) 68. doi:10.1140/epja/i2012-12068-7.

[17] B. L. Berman, R. E. Pywell, S. S. Dietrich, M. N. Thompson, K. G. McNeill, J. W. Jury, Absolute photoneutron cross sections for zr, i, pr, au, and pb, Physical Review C 36 (4) (1987) 1286–1292. doi:10.1103/PhysRevC.36.1286.

[18] S. C. Fultz, R. L. Bramblett, J. T. Caldwell, N. A. Kerr, Photoneutron cross-section measurements on gold using nearly monochromatic photons, Physical Review 127 (4) (1962) 1273–1279. doi:10.1103/PhysRev.127.1273.

[19] K. Y. Hara, H. Harada, F. Kitatani, S. Goko, S.-y. Hohara, T. Kaihori, A. Makinaga, H. Utsunomiya, H. Toyokawa, K. Yamada, Measurements of the ^{152} srn(γ,n) cross section with laser-compton scattering γ rays and the photon difference method, Journal of Nuclear Science and Technology 44 (7) (2007) 938–945. doi:10.1080/18811248.2007.9711333.

[20] O. Itoh, H. Utsunomiya, H. Akimune, T. Kondo, M. Kamata, T. Yamagata, H. Toyokawa, H. Harada, F. Kitatani, S. Goko, C. Nair, Y.-W. Lui, Photoneutron cross sections for au revisited: Measurements with laser compton scattering γ-rays and data reduction by a least-squares method, Journal of Nuclear Science and Technology 48 (5) (2011) 834–840. doi:10.1080/18811248.2011.9711766.

[21] F. Kitatani, H. Harada, S. Goko, H. Utsunomiya, H. Akimune, H. Toyokawa, K. Yamada, Measurement of ^{76} se and ^{78} se (γ, n) cross sections, Journal of Nuclear Science and Technology 48 (7) (2011) 1017–1024. doi:10.1080/18811248.2011.9711787.

[22] F. Kitatani, H. Harada, S. Goko, H. Utsunomiya, H. Akimune, T. Kaihori, H. Toyokawa, K. Yamada, Measurement of the ^{80} se(γ, n) cross section using laser-compton scattering γ-rays, Journal of Nuclear Science and Technology 47 (4) (2010) 367–375. doi:10.1080/18811248.2010.9711967.

[23] A. Veyssiere, H. Beil, R. Bergere, P. Carlos, A. Lepre-

tre, Photoneutron cross sections of 208pb and 197au, Nuclear Physics A 159 (2) (1970) 561–576. doi:10.1016/0375-9474(70)90727-X.

[24] K. Vogt, P. Mohr, M. Babilon, W. Bayer, D. Galaviz, T. Hartmann, C. Hutter, T. Rauscher, K. Sonnabend, S. Volz, A. Zilges, Measurement of the (γ, n) cross section of the nucleus 197au close above the reaction threshold, Nuclear Physics A 707 (1-2) (2002) 241–252. doi:10.1016/S0375-9474(02)00922-3.

[25] W. D. Bianco, S. Kundu, P. Boucher, ^{64}Zn(,n)^{63}Zn Cross Section From 20.4 to 21.9MeV, Canadian Journal of Physics 51 (12) (1973) 1302–1303. doi:https://doi.org/10.1139/p73-173.

[26] T. E. Rodrigues, J. D. T. Arruda-Neto, Z. Carvalheiro, J. Mesa, A. Deppman, V. P. Likhachev, M. N. Martins, Statistical and direct aspects of decay channels in the giant dipole resonance and quasideuteron energy regions, Physical Review C 68 (1) (2003) 014618. doi:10.1103/PhysRevC.68.014618.

[27] G. Hovhannisyan, T. Bakhshiyan, R. Dallakyan, Photonuclear production of the medical isotope 67Cu, Nuclear Instruments and Methods in Physics Research Section B: Beam Interactions with Materials and Atoms 498 (2021) 48–51. doi:10.1016/j.nimb.2021.04.016.

[28] A.M.Goryachev, G.N.Zalesnyy, The studying of the photoneutron reactions cross sections in the region of the giant dipole resonance in zinc,germanium, selenium, and strontium isotopes, Voprosy Teoreticheskoy i Yadernoy Fiziki 8 (121) (1982).

[29] T. Nakamura, K. Takamatsu, K. Fukunaga, M. Yata, S. Yasumi, Absolute Cross Sections of the (, n) Reaction for Cu^{63}, Zn^{64} and Ag^{109}, Journal of the Physical Society of Japan 14 (6) (1959) 693–698. doi:https://doi.org/10.1143/JPSJ.14.693.

[30] D. Owen, E. Muirhead, B. Spicer, Structure in the giant resonance of 64Zn and 63Cu, Nuclear Physics A 122 (1) (1968) 177–183. doi:https://doi.org/10.1016/0375-9474(68)90711-2.

[31] W. E. Del Bianco, W. E. Stephens, Photonuclear Activation by 20.5-Mev Gamma Rays, Physical Review 126 (2) (1962) 709–717. doi:10.1103/PhysRev.126.709.

[32] T. Kawano, Y. S. Cho, P. Dimitriou, D. Filipescu, N. Iwamoto, V. Plujko, X. Tao, H. Utsunomiya, V. Varlamov, R. Xu, R. Capote, I. Gheorghe, O. Gorbachenko, Y. L. Jin, T. Renstrom, M. Sin, K. Stopani, Y. Tian, G. M. Tveten, J. M. Wang, T. Belgya, R. Firestone, S. Goriely, J. Kopecky, M. Krticka, R. Schwengner, S. Siem, M. Wiedeking, IAEA Photonuclear Data Library 2019, Nuclear Data Sheets 163 (2020) 109–162. doi:10.1016/j.nds.2019.12.002.

[33] X. l. Huang, Nuclear Data Sheets for A = 196, Nuclear Data Sheets 108 (6) (2007) 1093–1286. doi:10.1016/j.nds.2007.05.001.

[34] A. Koning, D. Rochman, J.-C. Sublet, N. Dzysiuk, M. Fleming, S. van der Marck, Tendl: Complete nuclear data library for innovative nuclear science and technology, Nuclear Data Sheets 155 (2019) 1–55. doi:10.1016/j.nds.2019.01.002.

[35] M. Gai, M. W. Ahmed, S. C. Stave, W. R. Zimmerman, A. Breskin, B. Bromberger, R. Chechik, V. Dangendorf, T. Delbar, R. H. France, S. S. Henshaw, T. J. Kading, P. P. Martel, J. E. R. McDonald, P. N. Seo, K. Tittelmeier, H. R. Weller, A. H. Young, An optical readout tpc (o-tpc) for studies in nuclear astrophysics with gamma-ray beams at hiγs[1], Journal of Instrumentation 5 (12) P12004–P12004. doi:10.1088/1748-0221/5/12/P12004.

[36] M. Gai, D. Schweitzer, S. R. Stern, A. H. Young, R. Smith, M. Cwiok, J. S. Bihalowicz, H. Czyrkowski, R. Dabrowski, W. Dominik, A. Fijalkowska, Z. Janas, L. Janiak, A. Korgul, T. Matulewicz, C. Mazzocchi, M. Pfützner, M. Zaremba, D. Balabanski, I. Gheorghe, C. Matei, O. Tesileanu, N. V. Zamfir, M. W. Ahmed, S. S. Henshaw, C. R. Howell, J. M. Mueller, L. S. Myers, S. Stave, C. Sun, H. R. Weller, Y. K. Wu, A. Breskin, V. Dangendorf, K. Tittelmeier, M. Freer, Time projection chamber (tpc) detectors for nuclear astrophysics studies with gamma beams, Nuclear Instruments and Methods in Physics Research Section A: Accelerators, Spectrometers, Detectors and Associated Equipment 954 (2020) 161779. doi:10.1016/j.nima.2019.01.006.

[37] M. Gai, the UConn-Yale-Duke-Weizmann-PTB-UCL Collaboration, Studies in nuclear astrophysics with an optical readout tpc (o-tpc) at hi γ s, Journal of Physics: Conference Series 337 (2012) 012054. doi:10.1088/1742-6596/337/1/012054.

[38] A. Z. X. . W. H. Lv, , China Plant Engineering (23-25) (2022). doi:CNKI:SUN:SBGL.0.

[39] M. Arnould, S. Goriely, The p-process of stellar nucleosynthesis: Astrophysics and nuclear physics status, Physics Reports 384 (1-2) (2003) 1–84. doi:10.1016/S0370-1573(03)00242-4.

[40] K. Göbel, J. Glorius, A. Koloczek, M. Pignatari, R. Reifarth, R. Schach, K. Sonnabend, Nucleosynthesis simulations for the production of the p-nuclei^{92}mo and^{94}mo in a supernova type ii model, EPJ Web of Conferences 93 (2015) 03006. doi:10.1051/epjconf/20159303006.

[41] B. D. Fields, The primordial lithium problem, Annual Review of Nuclear and Particle Science 61 (1) (2011) 47–68. doi:10.1146/annurev-nucl-102010-130445.

[42] S. E. Woosley, T. A. Weaver, The evolution and explosion of massive stars. ii. explosive hydrodynamics and nucleosynthesis, The Astrophysical Journal Supplement Series 101 (1995) 181. doi:10.1086/192237.

[43] W. R. Zimmerman, M. W. Ahmed, B. Bromberger, S. C. Stave, A. Breskin, V. Dangendorf, T. Delbar, M. Gai, S. S. Henshaw, J. M. Mueller, C. Sun, K. Tittelmeier, H. R. Weller, Y. K. Wu, Unambiguous identification of the second 2+ state in 12c and the structure of the hoyle state, Physical Review Letters 110 (15) (2013) 152502. doi:10.1103/PhysRevLett.110.152502.

[44] R. Brun, F. Rademakers, Root — an object oriented data analysis framework, Nuclear Instruments and Methods in Physics Research Section A: Accelerators, Spectrometers, Detectors and Associated Equipment 389 (1-2) (1997) 81–86. doi:10.1016/S0168-9002(97)00048-X.

[45] N. Iwamoto, K. Kosako, T. Fukahori, JENDL photonuclear data file 2016, Journal of Nuclear Science and Technology 60 (8) (2023) 911–922. doi:10.1080/00223131.2022.2161657.